

## Calculated electrical and thermal resistivities of Nb and Pd

F. J. Pinski\*

State University of New York at Stony Brook, Stony Brook, New York 11794  
and Oak Ridge National Laboratory, Oak Ridge, Tennessee 37830

P. B. Allen

State University of New York at Stony Brook, Stony Brook, New York 11794

W. H. Butler

Oak Ridge National Laboratory, Oak Ridge, Tennessee 37830

(Received 31 December 1980)

The electrical and thermal resistivities ( $\rho$  and  $W$ ) of pure Nb and Pd are calculated from nearly first principles. Realistic Korringa-Kohn-Rostoker energy bands and wave functions, experimental phonon frequencies and Born-von Kármán eigenvectors, and rigid muffin-tin electron-phonon potentials are used to generate the velocities and scattering probabilities in the Bloch-Boltzmann equation, at a mesh of nearly 48 000 points on the Fermi surface. Solutions for  $\rho$  and  $W$  are exhibited at three levels of accuracy: (1) the lowest-order variational approximation (LOVA) where the Fermi surface displaces rigidly; (2) the  $N$ -sheet approximation where different sheets of Fermi surface displace independently; (3) a fully inelastic calculation where the  $N$ -sheet approximation is used and the distribution function is allowed arbitrary variations with energy (normal to the Fermi surface) to reflect the inelasticity of electron-phonon scattering. Above  $T = 100$  K, corrections to LOVA are of order 1%, but below  $T = 100$  K, both the  $N$ -sheet approximation and inelasticity give large corrections to the LOVA results. These results are also compared with Bloch-Grüneisen formulas fitted at  $T \sim \Theta_D$ . In the range  $100 \text{ K} \leq T \leq 300 \text{ K}$ , calculations exceed experimental results by  $\sim 10\%$ . Good agreement persists into the range  $10 \text{ K} \leq T \leq 100 \text{ K}$ , except that in Nb theory underestimates experiment significantly at the lower-temperature end, suggesting a possible error of rigid muffin-tin models for small  $Q$  scattering. In Pd the interpretation is complicated by Coulomb effects. Below  $T = 10$  K, finite mesh size prevents reliable calculations. Simple models such as Bloch-Grüneisen theory are inadequate to account for the data. Mott's (1936) "s-d" picture is shown to be qualitatively correct for Pd. Extension of this picture to Nb was suggested subsequently by various authors, but the present calculation does not support this.

### I. INTRODUCTION

The problem of electronic transport in metals was solved *in principle* over 50 years ago when Bloch<sup>1</sup> wrote down the semiclassical Boltzmann equation. *In practice*, there are still many features which are poorly understood. In particular, the understanding of transition metals<sup>2</sup> lags considerably behind that of "simple" metals.<sup>3</sup> The field retains a lively interest because transport properties, especially the electrical resistivity, are easily measured and carry important information about microscopic properties such as the electron-phonon interaction and the electron-electron interaction. In this paper, we investigate electron-phonon scattering in the transition metals Nb and Pd. Our objective is a realistic calculation which can be compared without adjustment to experimental measurements of electrical and thermal resistivities. We face two basic problems, first, generating the electronic velocities and scattering probabilities in the Boltzmann equation, and second, solving it.

First, it is necessary to know the electronic structure of the metal (at least in the vicinity of the Fermi energy), the phonon dispersion rela-

tions, and the electron-phonon matrix elements. Commonly used approximations such as spherical Fermi surfaces, Debye phonons, and electron-phonon matrix elements derived from screened pseudopotentials are inadequate for the transition metals. We use energy bands and wave functions generated by means of Korringa-Kohn-Rostocker (KKR) band theory. We use phonon dispersion curves and polarization vectors obtained from Born-von Kármán fits to neutron scattering experiments. For the electron-phonon matrix elements, we use the "rigid muffin-tin approximation" (RMTA).<sup>4</sup> This approximation (to be described in Sec. II B) is *ad hoc* but reasonable and has been shown to give good results for resistivity,<sup>2,5</sup> phonon linewidths,<sup>6-8</sup> and the electron-phonon mass enhancement<sup>4,9,10</sup> for transition metals. The use of the RMTA is the major approximation of this paper and agreement between theory and experiment provides a stringent test of the approximation.

To solve the Boltzmann equation, we use the Fermi-surface harmonic and energy polynomial formalisms developed by Allen<sup>11</sup> and Pinski.<sup>12</sup> These formalisms allow the Boltzmann equation (initially an integral equation in the wave vector)

to be written as a matrix equation which can be easily solved even for complicated materials such as Nb and Pd.

Overall, we obtain good agreement between theory and experiment and interpret this as a general confirmation of the rigid muffin-tin approximation. In Nb, however, in the temperature range of  $\sim 10$  to 20 K, our calculated resistivity is lower than experiment, which may indicate that the rigid muffin-tin matrix elements in Nb are too weak for small momentum transfer. A second important conclusion is that the lowest-order variational approximation<sup>11,13</sup> to the solution to the Boltzmann equation is inadequate at low temperatures. The experimental low-temperature electrical resistivity is often fitted to an expression of the form  $\rho = A + BT^2 + CT^3 + DT^5$ . The usual identification of the four terms with contributions from impurity, electron-electron, "s-d" electron-phonon, and "s-s" electron-phonon scattering seems to us flawed by serious ambiguity because the corrections from improved solutions of the Boltzmann equation are large and do not obey Mattheissen's rule.

To make contact with previous work, we present calculations performed at several levels of complexity. In Sec. II, we present calculations in the lowest-order variational approximation (LOVA) which show that the use of realistic phonons, energy bands, and matrix elements (as opposed to traditional approximations such as the Bloch-Grüneisen formula<sup>14</sup>) has a large effect on the temperature dependence of transport properties of transition metals. In Sec. III, we present more accurate solutions to the Boltzmann equation. These correction to LOVA become very important below about 40 K. In Sec. IV, we present a discussion of our results.

## II. LOWEST-ORDER VARIATIONAL APPROXIMATIONS

### A. Formalism

In the Boltzmann theory, the fundamental object is the electronic distribution function  $F_{\mathbf{k}}$ , which gives the number of electrons in quantum state  $\mathbf{k}$ . We use  $k$  as an abbreviated notation for the quantum numbers ( $\vec{k}n$ ), wave vector, and band index. In the absence of applied perturbations,  $F_{\mathbf{k}}$  is the Fermi function,  $f_{\mathbf{k}} = [\exp(\beta\epsilon_{\mathbf{k}}) + 1]^{-1}$ . The perturbations cause  $F_{\mathbf{k}}$  to deviate from  $f_{\mathbf{k}}$  for states near the Fermi surface,

$$F_{\mathbf{k}} = f_{\mathbf{k}} + \left( \frac{-\partial f}{\partial \epsilon_{\mathbf{k}}} \right) \phi_{\mathbf{k}}, \quad (1)$$

where energies are measured from the chemical potential  $\mu = \epsilon_F$ . This defines a smooth function

$\phi_{\mathbf{k}}$  which for weak perturbations is linear in the  $\vec{E}$  field or the thermal gradient  $\vec{\nabla}T$ .

From the distribution function, the currents can be calculated,

$$j_E = -2e \sum_{\mathbf{k}} v_{\mathbf{x}}(\mathbf{k}) \phi_{\mathbf{k}} \left( \frac{-\partial f}{\partial \epsilon_{\mathbf{k}}} \right) = \sigma E, \quad (2)$$

$$j_Q = 2 \sum_{\mathbf{k}} \epsilon_{\mathbf{k}} v_{\mathbf{x}}(\mathbf{k}) \phi_{\mathbf{k}} \left( \frac{-\partial f}{\partial \epsilon_{\mathbf{k}}} \right) = -\kappa \frac{dT}{dx}. \quad (3)$$

Here, we are taking the perturbing fields to lie in the  $x$  direction and assuming that the currents also lie in the  $x$  direction (as required by cubic symmetry). The electron velocity  $\vec{v}(\mathbf{k})$  is  $\vec{\nabla}_{\mathbf{k}}\epsilon_{\mathbf{k}}/\hbar$  and  $e$  is the magnitude of the electronic charge. In Eqs. (2) and (3), we are neglecting thermoelectric effects—the thermal current which accompanies the  $\vec{E}$  field and the electrical current which accompanies the thermal gradient. These are second-order effects which vanish in the model we use because we assume that within  $k_B T$  of the Fermi energy, the number of states, the electron velocities, and the scattering matrix elements are the same above as below the Fermi surface. Corrections to this approximation are of the order  $(k_B T/E_B)^2$  (where  $E_B$  is a "bandwidth" parameter) and can become important above room temperature. These corrections are called "Fermi smearing" effects, and we hope to deal with them in a later paper.

The distribution function  $\phi_{\mathbf{k}}$  is determined by the Boltzmann equation, which is known<sup>15</sup> to be valid if the mean free path  $l$  is longer than a few lattice constants. We neglect phonon drag, that is, the phonons are assumed to be in equilibrium. Thus the Boltzmann equation is

$$\left[ eE + \left( \frac{\epsilon_{\mathbf{k}}}{T} \right) \frac{dT}{dx} \right] v_{\mathbf{x}}(\mathbf{k}) \frac{\partial f}{\partial \epsilon_{\mathbf{k}}} = \sum_{\mathbf{k}'} Q_{\mathbf{k}\mathbf{k}'} \phi_{\mathbf{k}'}, \quad (4)$$

where  $Q_{\mathbf{k}\mathbf{k}'}$  is the scattering operator. Methods for solving Eq. (4) were given in Ref. 11. We rederive here some of the basic results in a less abstract way, hoping that this will clarify the results and clarify the way our calculations have been done. In particular, we find it helpful to make explicit the separation of  $Q_{\mathbf{k}\mathbf{k}'}$  into "scattering-out" and "scattering-in" terms,

$$Q_{\mathbf{k}\mathbf{k}'} = Q_{\mathbf{k}\mathbf{k}'}^{\text{out}} - Q_{\mathbf{k}\mathbf{k}'}^{\text{in}}, \quad (5)$$

each of which can be related to the equilibrium transition probability  $P_{\mathbf{k}\mathbf{k}'}$ :

$$Q_{\mathbf{k}\mathbf{k}'}^{\text{out}} = \frac{\delta_{\mathbf{k}\mathbf{k}'}}{k_B T} \sum_{\mathbf{k}''} P_{\mathbf{k}\mathbf{k}''}, \quad (6)$$

$$Q_{\mathbf{k}\mathbf{k}'}^{\text{in}} = \frac{1}{k_B T} P_{\mathbf{k}\mathbf{k}'}. \quad (7)$$

Formally, the distribution function can be ob-

tained by solving Eq. (4),

$$\phi_k = \sum_{k'} [Q^{-1}]_{kk'} \left[ eE + \left( \frac{\epsilon_{k'}}{T} \right) \frac{dT}{dx} \right] v_x(k') \frac{\partial f}{\partial \epsilon_{k'}}, \quad (8)$$

but in practice, inversion of the scattering operator is difficult. Fortunately, there is a variational principle<sup>13</sup> which allows the currents (2) and (3) to be computed by adjusting trial functions  $\phi_k^\dagger$ . This technique has the advantage that if  $\phi_k^\dagger$  differs from  $\phi_k$  by an amount of order  $\epsilon$ , then the currents will differ from the exact results by amounts of order  $\epsilon^2$ . In this section, we use approximate trial functions  $\phi_k^{(E,0)}$  and  $\phi_k^{(Q,0)}$ , which are the simplest sensible trial functions for the cases of applied electrical fields and thermal gradients, respectively,

$$\phi_k^{(E,0)} = -eE v_x(k) \tau_E, \quad (9)$$

$$\phi_k^{(Q,0)} = \left( -\frac{dT}{dx} \right) \left( \frac{\epsilon_k}{T} \right) v_x(k) \tau_Q. \quad (10)$$

Since  $\phi$  has units of energy [Eq. (1)],  $\tau_E$  and  $\tau_Q$  must have units of time. The variational method yields specific equations for  $\tau_E$  and  $\tau_Q$  which we will present shortly. Equations (9) and (10) can be interpreted as meaning that when an  $E$  field is applied, the Fermi distribution is rigidly shifted by an amount  $\delta_k = -eE\tau_E/\hbar$ , or when a thermal gradient is applied it is shifted nonrigidly (because of the  $k$  dependence of  $\epsilon_k$ ) by an amount  $(-dT/dx)(\epsilon_k/T)\tau_Q/\hbar$ . We are interested in wave vectors near the Fermi surface and use a coordinate system in which a point is described by its position on the Fermi surface ( $\vec{k}_{FS}$ ) and its distance  $\epsilon_k$  above (or below) the Fermi surface. In terms of this coordinate system, both of the above shifts  $\delta_k$  of the distribution function are independent of ( $\vec{k}_{FS}$ ) but the second is proportional to  $\epsilon_k$ .

The resulting LOVA formulas for the conductivities  $\sigma$  and  $\kappa$  are

$$\sigma^{(0)} = 2N(0)\langle v_x^2 \rangle e^2 \tau_E, \quad (11)$$

$$\kappa^{(0)} = 2N(0)\langle v_x^2 \epsilon^2 \rangle \tau_Q / T, \quad (12)$$

where the band averages in Eqs. (11) and (12) are defined by

$$N(0)\langle v_x^2 \rangle \equiv \sum_k v_x^2(k) \left( \frac{-\partial f}{\partial \epsilon_k} \right) \cong \sum_k v_x^2(k) \delta(\epsilon_k), \quad (13)$$

$$\begin{aligned} N(0)\langle v_x^2 \epsilon^2 \rangle &\equiv \sum_k v_x^2(k) \epsilon_k^2 \left( \frac{-\partial f}{\partial \epsilon_k} \right) \\ &\cong \frac{1}{3} (\pi k_B T)^2 \sum_k v_x^2(k) \delta(\epsilon_k). \end{aligned} \quad (14)$$

The final forms of Eqs. (13) and (14) neglect "Fermi smearing." In this approximation, the Lorenz number defined by  $L = \kappa/\sigma T$  is  $L = L_0 \tau_Q/\tau_E$ , where  $L_0 = \pi^2 k_B^2/3e^2$ . The Lorenz number takes the Sommerfeld value  $L_0$  if the "relaxation times"  $\tau_Q$  and  $\tau_E$  are equal. In general, these are unequal, but, if inelastic scattering effects are unimportant (i.e., if impurity scattering dominates or if the energy gained or lost by absorbing or emitting a phonon is smaller than  $k_B T$ ), then  $\tau_Q$  and  $\tau_E$  are equal<sup>14</sup> in LOVA.

It is now simple to solve Eq. (4) for  $\tau_E$  or  $\tau_Q$  by substituting  $\phi_k$  [Eqs. (9) or (10)] and operating on both sides of Eq. (4) with  $\sum_k v_x(k)$  for the case of an applied  $\vec{E}$  field or  $\sum_k v_x(k) \epsilon_k$  for the case of a thermal gradient. Using Eqs. (6) and (7), the results for either  $\tau_E$  or  $\tau_Q$  can be expressed as a "scattering-out" term minus a "scattering-in" term,

$$\frac{1}{\tau_{E[Q]}} = \left( \frac{1}{\tau_{E[Q]}} \right)^{\text{out}} - \left( \frac{1}{\tau_{E[Q]}} \right)^{\text{in}}, \quad (15)$$

$$\left( \frac{1}{\tau_{E[Q]}} \right)^{\text{out(in)}} = \sum_{kk'} \frac{P_{kk'} v_x(k) v_x(k') [\epsilon_k \epsilon_{k'}]}{k_B T N(0) \langle v_x^2 [\epsilon^2] \rangle}, \quad (16)$$

where the notation means that the parenthetical primes on the argument of  $v_x$  and on the subscript of  $\epsilon$  are to be omitted for the "out" lifetimes and the square brackets enclosing two factors of energy are to be replaced by 1 for the  $\vec{E}$ -field lifetime. At high temperatures or for reasonably isotropic impurity scattering  $(1/\tau_{E[Q]})^{\text{in}}$  is small compared to  $(1/\tau_{E[Q]})^{\text{out}}$  because the average of  $v_x(k)$  over the Fermi surface is zero. For phonon scattering at low temperatures, on the other hand,  $P_{kk'}$  is small unless  $k \approx k'$  and so the "out" and "in" terms are comparable,  $(1/\tau_{E[Q]})^{\text{out}} \gtrsim (1/\tau_{E[Q]})^{\text{in}}$ .

For phonon scattering,  $P_{kk'}$  has the form

$$P_{kk'} = \frac{2\pi}{\hbar} \sum_j |M_{kk'}^j|^2 g(\epsilon_k, \epsilon_{k'}, \omega_{k-k}^j), \quad (17a)$$

$$\begin{aligned} g(\epsilon, \epsilon', \omega) &= f(\epsilon)[1 - f(\epsilon')] \\ &\times \{ N(\omega) \delta(\epsilon - \epsilon' + \hbar\omega) \\ &+ [N(\omega) + 1] \delta(\epsilon - \epsilon' - \hbar\omega) \}, \end{aligned} \quad (17b)$$

where  $M_{kk'}^j$  is the electron-phonon matrix element for scattering between Bloch states  $k$  and  $k'$  due to a phonon of polarization index  $j$ , and  $N(\omega)$  is a Bose factor  $N(\omega) = [e^{\beta\hbar\omega} - 1]^{-1}$ . The various lifetimes (16) can be written using (17) in the form

$$\left( \frac{1}{\tau_{E[Q]}} \right)^{\text{out(in)}} = \frac{\Omega_n^2}{\hbar(2\pi)^5} \int d\epsilon' \int d\epsilon'' \int_{\epsilon'} \frac{dS_k}{\hbar v_k} \int_{\epsilon''} \frac{dS_{k'}}{\hbar v_{k'}} \sum_j |M_{kk'}^j|^2 v_x(k) v_x(k'') g(\epsilon, \epsilon', \omega_{k-k}^j) [\epsilon \epsilon''] / k_B T N(0) \langle v_x^2 [\epsilon^2] \rangle. \quad (18)$$

where  $\Omega_a$  is the volume per atom and  $dS_k$  is an element of Fermi-surface area. At this stage, it is convenient to neglect "Fermi smearing" because this allows the surface integrals velocities and matrix elements to be evaluated at the Fermi energy. Then the integrals over  $\epsilon$  and  $\epsilon'$  may be performed analytically and independently of the surface integrals,

$$G_{E[Q]}^{\text{out(in)}}(\omega) = \frac{\hbar\omega}{2(k_B T)^2} \int_{-\infty}^{\infty} d\epsilon \int_{-\infty}^{\infty} d\epsilon' g(\epsilon, \epsilon', \omega) \left[ \frac{3\epsilon\epsilon'}{\pi^2(k_B T)^2} \right]. \quad (19)$$

The various  $G$ 's depend only on  $x = \hbar\omega/2k_B T$ ,

$$G_E^{\text{out}} = G_E^{\text{in}} = x^2/\sinh^2 x, \quad (20)$$

$$G_Q^{\text{out}} = (x^2/\sinh^2 x)(1 + 4x^2/\pi^2), \quad (21)$$

$$G_Q^{\text{in}} = (x^2/\sinh^2 x)(1 - 2x^2/\pi^2). \quad (22)$$

The surface integrals can now be evaluated and written in terms of transport spectral functions  $\alpha^2(\omega)F(\omega)$  which are analogs of the electron-phonon spectral function of the superconductivity theory.<sup>16</sup> A factor  $1 = \int d\omega \delta(\omega - \omega_{k-k'})$  is inserted into Eq. (18), yielding

$$\left( \frac{1}{T_{E[Q]}} \right)^{\text{out(in)}} = \frac{2\pi k_B T}{\hbar} 2 \int \frac{d\omega}{\omega} \alpha_{\text{out(in)}}^2(\omega) F(\omega) G_{E[Q]}^{\text{out(in)}}(x), \quad (23)$$

$$\alpha_{\text{out(in)}}^2(\omega) F(\omega) = \left( \frac{\Omega_a^2}{(2\pi)^6} \int \frac{dS_k}{\hbar v_k} \int \frac{dS_{k'}}{\hbar v_{k'}} \sum_j |M_{kk'}^j|^2 v_x(k) v_x(k') \delta(\omega - \omega_{k-k'}) \right) / \hbar N(0) (v_x^2). \quad (24)$$

In cubic systems,  $v_x(k) v_x(k')$  may be replaced by  $\frac{1}{3} \vec{v}(k) \cdot \vec{v}(k')$ . The difference between the out and in spectral functions is often called the transport spectral function and denoted<sup>11</sup>  $\alpha_{\text{tr}}^2(\omega)F(\omega)$  or  $\alpha^{2(+xx)}F(\omega)$ ,

$$\alpha_{\text{tr}}^2(\omega)F(\omega) = \alpha_{\text{out}}^2(\omega)F(\omega) - \alpha_{\text{in}}^2(\omega)F(\omega). \quad (25)$$

Generally,  $\alpha_{\text{out}}^2 F(\omega)$  is much greater than  $\alpha_{\text{in}}^2 F(\omega)$  except at low frequencies where  $\alpha_{\text{in}}^2 F(\omega)$  nearly cancels  $\alpha_{\text{out}}^2 F(\omega)$  and converts the  $\omega^2$  dependence of the individual parts into an  $\omega^4$  variation of  $\alpha_{\text{tr}}^2 F(\omega)$  (see Fig. 1).

Closed-form LOVA expressions for the electrical and thermal resistivities result from Eqs. (11) and (12) and (20)–(24),

$$\rho^{(0)} = \frac{2\pi k_B T}{e^2 \hbar N(0) (v_x^2)} \int_0^\infty \frac{d\omega}{\omega} \frac{x^2}{\sinh^2 x} \alpha_{\text{tr}}^2(\omega) F(\omega), \quad (26)$$

$$W^{(0)} = \frac{6}{\pi \hbar k_B N(0) (v_x^2)} \int_0^\infty \frac{d\omega}{\omega} \frac{x^2}{\sinh^2 x} \left( \alpha_{\text{tr}}^2(\omega) F(\omega) + \frac{4x^2}{\pi^2} \alpha_{\text{out}}^2(\omega) F(\omega) + \frac{2x^2}{\pi^2} \alpha_{\text{in}}^2(\omega) F(\omega) \right). \quad (27)$$

Again by analogy with superconducting notation, we define parameters  $\lambda_r$  and  $(\omega^2)_r$ ,

$$\lambda_r \equiv 2 \int_0^\infty \frac{d\omega}{\omega} \alpha_r^2(\omega) F(\omega), \quad (28)$$

$$\lambda_r(\omega^2)_r \equiv 2 \int_0^\infty d\omega \omega \alpha_r^2(\omega) F(\omega), \quad (29)$$

where  $r$  stands for in, out, or tr. The parameter  $\lambda_{\text{tr}} = \lambda_{\text{out}} - \lambda_{\text{in}}$  is the transport analog of the dimensionless parameter  $\lambda$  which determines the superconducting transition temperature  $T_c$ .<sup>17</sup> An important conclusion of our work is that  $\lambda_{\text{tr}}$  agrees with  $\lambda$  to about 10% for Nb and Pd when both are calculated by our procedures. It seems probable that the result  $\lambda_{\text{tr}} \simeq \lambda$  is typical of  $d$ -band metals.

In the high-temperature (small- $x$ ) limit, Eqs. (26) and (27) become

$$\rho^{(0)} = \frac{2\pi k_B T / \hbar}{2N(0) (v_x^2)} \lambda_{\text{tr}} \left[ 1 - \frac{\hbar^2 (\omega^2)_{\text{tr}}}{12 k_B^2 T^2} + \dots \right], \quad (30)$$

$$W^{(0)} = \frac{6/\pi k_B \hbar}{2N(0) (v_x^2)} \left[ \lambda_{\text{tr}} + \frac{\hbar^2}{k_B^2 T^2} \left( \frac{\lambda_{\text{out}}(\omega^2)_{\text{out}}}{\pi^2} + \frac{1}{2\pi^2} \lambda_{\text{in}}(\omega^2)_{\text{in}} - \frac{\lambda_{\text{tr}}(\omega^2)_{\text{tr}}}{12} \right) + \dots \right]. \quad (31)$$

Thus, within LOVA, the Lorenz number approaches the Sommerfeld value when the thermal energy exceeds a typical phonon energy  $T \gtrsim \Theta_D$ .

Equations (26) and (27) are modern versions of

equations derived earlier by Bloch<sup>18</sup> and by Wilson,<sup>19</sup> respectively, generalized<sup>11</sup> to include realistic energy bands, phonons, and electron-phonon matrix elements. The equations of Bloch and

Wilson are familiar from textbooks,<sup>13,14</sup> the former being called Bloch-Grüneisen theory. To make contact with these equations, it is necessary to recall that they are based on a model employing Debye phonons, a spherical Fermi surface and deformation-potential electron-phonon coupling via longitudinal phonons only, with no umklapp scattering. In this model the matrix elements  $|M_{kk'}^j|^2$  in Eq. (24) are replaced by  $Cq^2/\omega$  for the longitudinal modes and zero for the transverse modes where  $C$  is a constant and  $q = k' - k$ . Because of the assumption of a spherical Fermi surface, the factor  $v^2(k)$  can be replaced by a constant  $v_F^2$  and  $\vec{v}(k) \cdot \vec{v}(k')$  can be replaced by  $v_F^2(\hat{k} \cdot \hat{k}')$ . The integrals over solid angles can be performed by writing the delta function as

$$\delta(\omega - S|\vec{k}' - \vec{k}|) = \frac{\omega}{k_F^2 S^2} \delta\left(\hat{k} \cdot \hat{k}' - 1 + \frac{\omega^2}{2k_F^2 S^2}\right), \quad (32)$$

where  $S$  is the sound velocity and  $k_F$  is the Fermi wave number. The results can be written as

$$\alpha_{\text{tr}}^2(\omega)F(\omega) - 2\lambda_{\text{tr}}(\omega/\omega_D)^4, \quad (34)$$

$$\alpha_{\text{out}}^2(\omega)F(\omega) - \lambda_{\text{tr}}(\omega/\omega_D)^2(2k_F/q_D)^2, \quad (33)$$

$$\alpha_{\text{in}}^2(\omega)F(\omega) - \lambda_{\text{tr}}(\omega/\omega_D)^2[(2k_F/q_D)^2 - 2\omega^2/\omega_D^2], \quad (35)$$

where  $\omega_D$  and  $q_D$  are the Debye frequency and wave number, respectively. Using these spectral functions, we recover the traditional formulas which depend on three constants  $\rho' = 2\pi k_B \lambda_{\text{tr}} / [2e^2 N(0)(v_x^2)]$ ,  $\Theta = \hbar\omega_D/k_B$ , and  $k_F/q_D$ ,

$$\rho_{\text{BG}}(T) = 4\rho'T(T/\Theta)^4 J_5(\Theta/T), \quad (36)$$

$$W_{\text{BG}}(T) = (4\rho'/L_0)(T/\Theta)^4 \times \left\{ [1 + (3/\pi^2)(k_F/q_D)^2(\Theta/T)^2] J_5(\Theta/T) - (1/2\pi^2) J_7(\Theta/T) \right\}, \quad (37)$$

where

$$J_n(\Theta/T) = 2^{n-1} \int_0^{\Theta/2T} dx x^{n-2} \frac{x^2}{\sinh^2 x}. \quad (38)$$

The label BG on  $\rho$  and  $W$  [Eqs. (36) and (37)] stands for Bloch-Grüneisen. In the case of  $W$ , this is unfair to Wilson, but the notation  $W_w$  seems unsatisfactory. Although these equations are based on a highly oversimplified model, they capture the correct trends of temperature dependence. In Sec. IIC, we shall show the results of these simple models are altered by the use of more realistic energy bands, phonon frequencies, and matrix elements.

#### B. Computational details

The core of our work is a careful evaluation of the spectral functions (24). The basic procedures have already been discussed<sup>7</sup> in the context of calculations of the closely related properties  $\gamma_q^j$  (the decay rate of a phonon into electron-hole pairs) and  $\alpha^2(\omega)F(\omega)$  (the spectral function which determines the  $T_c$  of superconductors). Equations (1.18), (1.12), and (1.13) of Ref. 7 need only be generalized in a straightforward way to include the velocity factors  $v_x(k)v_x(k')$ :

$$\alpha_{\text{out}}^2(\text{in})(\omega)F(\omega) = \frac{\Omega_a}{(2\pi)^3 2M\omega} \int d^3q \sum_{\alpha\beta j} \epsilon_\alpha^j(q) \epsilon_\beta^j(q) \delta(\omega - \omega_q^j) \eta_{\alpha\beta}^{\text{out}(\text{in})}(q), \quad (39)$$

$$\eta_{\alpha\beta}^{\text{out}(\text{in})}(q) = \frac{\Omega_a}{(2\pi)^3 N(0)(v_x^2)} \int \frac{dS_k}{\hbar v_k} \int \frac{dS_{k'}}{\hbar v_{k'}} \langle \psi_k | \hat{x}_\alpha \cdot \nabla V | \psi_{k'} \rangle \langle \psi_{k'} | \hat{x}_\beta \cdot \nabla V | \psi_k \rangle v_x(k) v_x(k') \delta(k - k' - q) \quad (40)$$

Just as in Refs. 7 and 8, the wave functions and Fermi velocities were generated on a dense mesh at the Fermi energy (676 × 48 points for Pd, 1071 × 48 points for Nb) using constant-energy search KKR techniques.<sup>20,21</sup> The double Fermi-surface integrals of Eq. (40) were evaluated, and the results  $\eta_{\alpha\beta}^{\text{out}(\text{in})}(q)$  were stored and subsequently plugged into Eq. (39) which was evaluated using a Gilat-Raubenheimer technique.<sup>22</sup> The potentials used to calculate the wave functions, Fermi surfaces, and Fermi velocities have been described previously. The potential of Nb ( $V_2$  of Ref. 7) was adjusted slightly to achieve better agreement with de Haas-van Alphen data.<sup>23</sup> The phonon frequencies and polarization vectors  $\omega_q^j$  and  $\epsilon_q^j$  come from Born-von Kármán fits<sup>24,25</sup> to neutron scattering experiments and are calculated on a Gilat-Rauben-

heimer mesh which subdivides the zone-boundary wave vector in the  $x$  direction into 24 bins. Each electronic scattering event  $\vec{k} - \vec{k}'$  then corresponds to some  $q$  bin from which the corresponding  $\omega_{k-k'}^j$  and  $\epsilon_{k-k'}^j$  are taken. This procedure leads to random errors in the spectral functions (39) which are statistically unimportant except at low  $\omega$  where the number of bins gets small. Thus, the low- $\omega$  tail of the spectral function has a relatively large random error, leading to unreliable results in  $\sigma(T)$  below a temperature of order  $\Theta_p/24$  or ~10 K. Therefore, we have calculated transport coefficients only for  $T > 10$  K.

The only aspect in which our work deviates from rigorous one-electron theory is in the use of the RMTA in calculating the matrix elements of Eq. (40). The RMTA is the assumption that when an

atom in a crystal is displaced its (KKR or augmented plane-wave) muffin-tin potential displaces rigidly with it. This is an approximation because it does not correctly account for the redistribution of the electron density which will occur in the real solid. It seems, however, not to be a bad approximation for a transition metal where the  $d$  electrons are rather tightly bound to the nucleus and where charge fluctuations are screened out rapidly because of the high Fermi energy density of states. It has worked well in previous electron-phonon calculations for the transition metals.<sup>4-10</sup>

### C. LOVA results

Figure 1 shows the transport spectral functions which we have calculated for Nb and for Pd, and

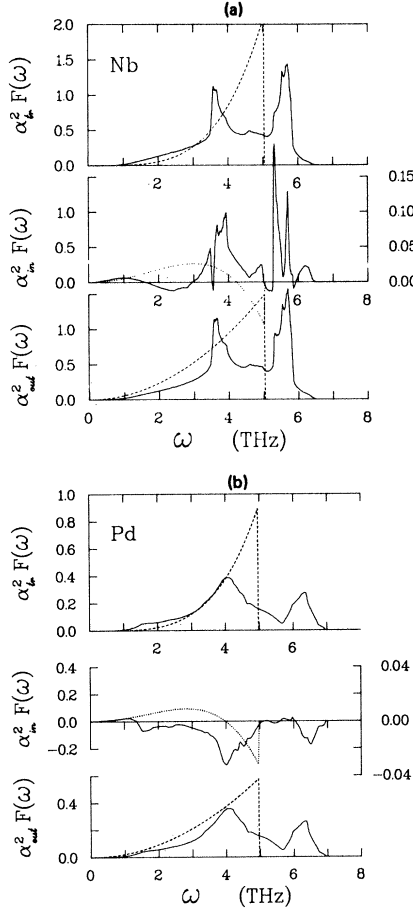


FIG. 1. Spectral functions for Nb and Pd. The solid curves denote spectral functions calculated using realistic phonons, energy bands, and matrix elements. The dashed and dotted curves are “Bloch-Grüneisen” analogs of the realistic spectral functions. The upper panels show  $\alpha_{tr}^2(\omega)F(\omega)$  which is the difference between the spectral functions in the bottom [ $\alpha_{out}^2(\omega)F(\omega)$ ] panels. Note the change of scale for  $\alpha_{in}^2(\omega)F(\omega)$ .

compares them with the corresponding spherical (Debye) models [Eqs. (33)–(35)]. The coefficients of the spherical models  $\lambda_{tr}$ ,  $\omega_D$ , and  $k_F/q_D$  are tabulated in Table I. The coefficients were chosen so that the spherical models would be in agreement with the calculated LOVA results at high temperature through terms of order  $\langle\omega^2\rangle/T^2$  [see Eqs. (30), (31), (36), and (37)]. This procedure leads to the identifications  $\omega_D = (3\langle\omega^2\rangle_{tr}/2)^{1/2}$  and  $k_F/q_D = (\lambda_{out}\langle\omega^2\rangle_{out}/3\lambda_{tr}\langle\omega^2\rangle_{tr})^{1/2}$ .

Figure 2 shows  $\rho/T$  calculated in the two approximations for Nb and for Pd. A detailed comparison of theory with experiment is postponed until Sec. IV. The point we wish to make here is that use of more realistic energy bands, matrix elements, and phonon frequencies alters the frequency dependence of the spectral functions and that this alteration shows up in the temperature dependence of the transport coefficients.

The values of  $\rho/T$  calculated using the more realistic spectral functions are larger at low  $T$  than those calculated using the simple model because the calculated  $\alpha_{tr}^2(\omega)F(\omega)$  is larger at low  $\omega$  than  $2\lambda_{tr}(\omega/\omega_D)^4$ . This result should not be surprising; a similar effect occurs in the lattice specific heat and has been known for some time. The phonon density of states is not proportional to the Debye density of states  $F_D(\omega) = 9\omega^2\Theta(\omega_D - \omega)/\omega_D^3$  except at very low frequencies. The true density of states quickly rises above its limiting  $\omega^2$  behavior because the phonon dispersion curves typically have a negative curvature. Consequently, if  $\omega_D$  is chosen to produce the correct lattice specific heat at high  $T$ , the Debye formula will underestimate the lattice specific heat at low  $T$ . This is why  $\Theta_D(T)$  obtained by setting the Debye formula equal to the observed lattice specific heat typically decreases as the temperature is lowered. The discrepancy between  $\rho_{BG}$  and  $\rho_{LOVA}$  is larger than that between the Debye and experimental lattice specific heats because the approximation for the matrix elements  $|M_{kk'}^i|^2 \sim C(k - k')^2/\omega_{k-k'}^4$  breaks down for relatively small values of  $q = k - k'$  in the transition metals. It is unlikely that a true Bloch-Grüneisen  $T^5$  term in the electrical resistivity has ever been observed in a transition metal. The resistivity calculated from Eq. (26) varies as  $T^5$  only at very low temperatures  $\lesssim 5$  K for Nb and Pd. The  $T^5$  coefficients reported in the literature typically are observed at higher temperatures and probably result from deviations of the resistivity from Eq. (26) which arise from the wave vector and energy dependence of the distribution function as described in Sec. III.

Figure 3 shows the thermal resistivity (multiplied by the Sommerfeld value of the Lorenz number  $L_0$ ) calculated using the realistic spectral

TABLE I. Calculated transport parameters of Nb and Pd. The Fermi-energy density of states  $N(0)$  and the root-mean-square Fermi velocity  $(\langle v^2 \rangle)^{1/2}$  were calculated from the band structures. The various  $\lambda$ 's and  $\langle \omega^2 \rangle_{tr}$  were calculated from the relevant spectral functions. The final three parameters give the Bloch-Grüneisen-Wilson fits of Eqs. (36) and (37).

	Nb	Pd
$N(0)$ (states/Ry atom spin)	9.9	15.5
$(\langle v^2 \rangle)^{1/2}$ (cm/s)	$6.1 \times 10^7$	$3.3 \times 10^7$
$\lambda$	1.118	0.41
$\lambda_{tr}$	1.073	0.461
$\lambda_{out}$	1.128	0.442
$\lambda_{in}$	0.055	-0.019
$\hbar \langle \omega^2 \rangle_{tr}^{1/2} / k_B$ (K)	197.6	195.7
$\hbar \langle \omega^2 \rangle_{out}^{1/2} / k_B$ (K)	197.7	195.1
$\rho'$ ( $\mu\Omega$ cm/K)	0.0550	0.0407
$\Theta_D$ (K)	242.0	239.7
$k_F / q_D$	0.592	0.564

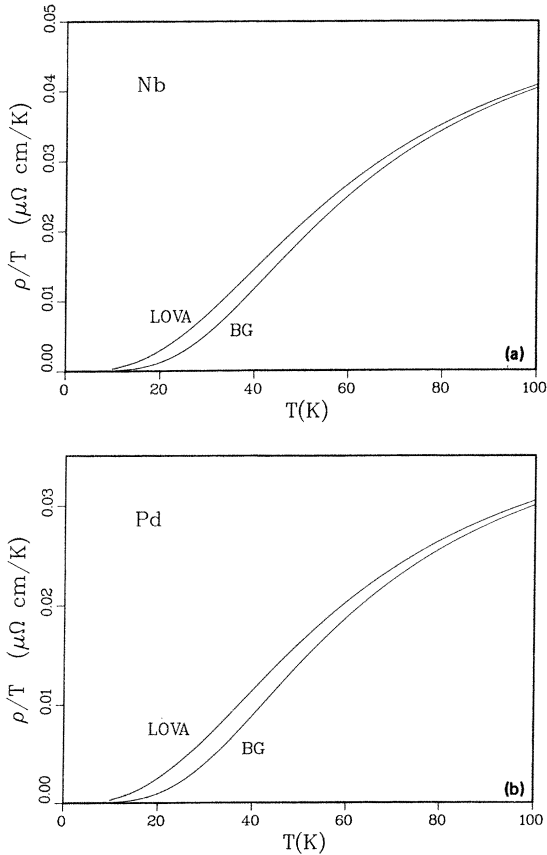


FIG. 2. Electrical resistivity divided by temperature for Nb and Pd in the lowest-order variational approximation. The curves labeled LOVA were calculated using the realistic forms of  $\alpha_{tr}^2(\omega)F(\omega)$  shown in Fig. 1. The curves labeled BG were calculated using the Bloch-Grüneisen form of the transport spectral function (also shown in Fig. 1).

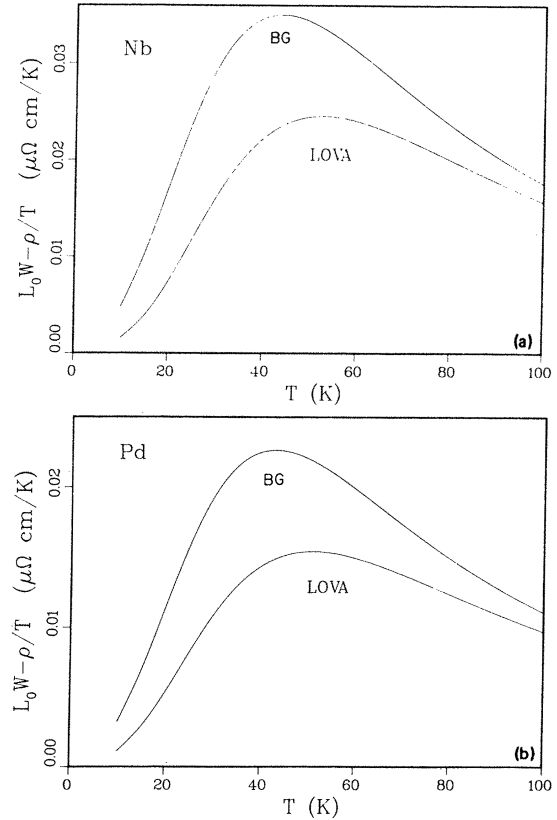


FIG. 3. Thermal resistivity of Nb and Pd in the lowest-order variational approximation. That component of the thermal resistivity,  $W$ , which satisfies the Wiedemann-Franz law has been subtracted. The curve labeled LOVA was calculated using the realistic versions of  $\alpha_{out}^2(\omega)F(\omega)$  and  $\alpha_{in}^2(\omega)F(\omega)$ . The curves labeled BG were calculated using the Bloch-Grüneisen analogs of these spectral functions.

functions and using the simple model. In order to emphasize the temperature variation not contained in the resistivity we have subtracted out  $\rho/T$ , that part of the thermal resistivity which obeys the Wiedeman-Franz law. The Wilson formula is substantially above the more realistic LOVA results below 100 K because  $\alpha_{\text{out}}^2(\omega)F(\omega)$  is substantially larger at low  $\omega$  in the Wilson model than in the more realistic calculation.

### III. BEYOND LOVA

#### A. Formalism

In this section, we show how to obtain a better solution to the Boltzman equation by allowing wave-vector and energy dependence of the distribution function. We also derive expressions for the electrical and thermal conductivities which are computationally convenient for transition metals. These expressions are slight modifications of the results of Allen<sup>11</sup> and Pinski.<sup>12</sup>

Following Ref. 11, we expand the distribution function in terms of functions  $F_j(k, \epsilon)$  and  $\sigma_n(\epsilon)$ ,

$$\phi_k = \sum_{nj} \phi_{nj} F_j(k, \epsilon) \sigma_n(\epsilon). \quad (41)$$

The functions  $F_j(k, \epsilon)$  are orthonormal over a constant energy surface of energy  $\epsilon$ ,

$$\sum_k F_j(k, \epsilon) F_{j'}(k, \epsilon) \delta(\epsilon_k - \epsilon) / \sum_k \delta(\epsilon_k - \epsilon) = \delta_{jj'}, \quad (42)$$

and are used to describe the variation of  $\phi_k$  from point to point on this surface. The functions  $\sigma_n(\epsilon)$ , on the other hand, are orthonormal with weighting function  $(-\partial f / \partial \epsilon)$ ,

$$\int_{-\infty}^{\infty} d\epsilon \left( -\frac{\partial f}{\partial \epsilon} \right) \sigma_n(\epsilon) \sigma_{n'}(\epsilon) = \delta_{nn'}, \quad (43)$$

and are used to describe the variations of  $\phi_k$  in directions normal to a constant energy surface. From Eq. (17b) it is clear that the transitions caused by the scattering operator occur between states within  $\pm k_B T$  of the Fermi energy. In this paper, we are interested in temperatures of several hundred degrees Kelvin or less. Over this energy range, the topology of the constant energy surface of a typical metal does not change appreciably so that we need only evaluate the functions  $F_j(k, \epsilon)$  at the Fermi energy. Consequently, we omit the  $\epsilon$  variable  $F_j(k, \epsilon) \rightarrow F_j(k)$ . If Fermi smearing is neglected, Eqs. (42) and (43) can be combined to yield the orthogonality relation

$$\sum_k F_j(k) \sigma_n(\epsilon_k) F_{j'}(k) \sigma_{n'}(\epsilon_k) \left( -\frac{\partial f}{\partial \epsilon_k} \right) = N(0) \delta_{nn'} \delta_{jj'}. \quad (44)$$

Several choices are available for the functions

$F_j(k)$ . Allen suggested orthogonal polynomials in the Fermi velocity (which he called Fermi-surface harmonics) and showed that only functions with  $\Gamma_{15}$  symmetry need be considered for a cubic system since  $\phi_k$  must have this symmetry. Unfortunately, Khan and Allen<sup>26</sup> have recently found that Fermi-surface harmonics constructed in this way are not suitable for expanding the  $\Gamma_1$  function  $\lambda_k$  (mass enhancement) because of slow convergence. Polynomials in the wave-vector components appeared to give better convergence in their tests. Convergence studies of  $\phi_k$  have not yet been made.

The calculations to be described below were performed using first-order Fermi-surface harmonics in the "disjoint representation," that is,

$$F_j(k) = v_x(k) \delta_j(k) / v_j, \quad (45)$$

where  $\delta_j(k)$  is unity for  $k$  on sheet  $j$  of the Fermi surface and zero elsewhere. The coefficient  $v_j^{-1}$  is chosen so that Eq. (42) is satisfied,

$$v_j = \left( \frac{N_j(0) \langle v_{xj}^2 \rangle}{N(0)} \right)^{1/2}, \quad (46)$$

where  $N_j(0) \langle v_{xj}^2 \rangle$  is identical to the quantity defined in Eq. (13) except that the Fermi-surface integral implied by Eq. (13) is restricted to sheet  $j$  of the Fermi surface. The coefficients  $v_j$  have the useful property  $\sum_j v_j^2 = \langle v_x^2 \rangle$ . An expansion of  $\phi_k$  in the basis of Eq. (45) amounts to a generalization of Eqs. (9) and (10) to allow different relaxation times on each sheet of the Fermi surface.

The choice of the functions  $\sigma_n(\epsilon)$  is also somewhat arbitrary. Allen suggested orthogonal polynomials in  $\epsilon$ ,

$$\sigma_n(\epsilon) = (2n+1)^{1/2} \sum_{m=0}^n C_{nm} \left( \frac{\epsilon}{2\pi k_B T} \right)^m, \quad (47)$$

where the coefficients  $C_{nm}$  are chosen so that Eq. (43) is satisfied. They can be obtained from a recursion relation given in Ref. 11. The first two of these polynomials are  $\sigma_0 = 1$ ,  $\sigma_1 = \sqrt{3\epsilon} / \pi k_B T$ . Another possible choice is the set of Legendre polynomials with argument  $\tanh(\epsilon / 2k_B T)$ ,

$$\sigma_n(\epsilon) = (2n+1)^{1/2} P_n(\tanh \epsilon / 2k_B T). \quad (48)$$

These functions satisfy Eq. (43) automatically, and have been used by Engquist<sup>27</sup> to study  $\sigma(T)$ . Pinski<sup>12</sup> found that the set equation (48) gives a very rapid convergence for the ideal thermal conductivity at low  $T$  but that the polynomials in  $\epsilon$  [Eq. (47)] gave better results at high  $T$ . A mixed basis,  $1$ ,  $\tanh \epsilon / 2k_B T$  and higher-order polynomials in  $\epsilon$  gave good results at all temperatures.

The calculations to be described below employed

the polynomials in  $\epsilon$  [Eq. (47)] together with a continued-fraction extrapolation to approximate the limit of an infinite number of polynomials. This extrapolation procedure was found<sup>12</sup> to be satisfactory [when using the basis set of Eq. (47)] for getting the correct thermal resistivity at low temperature.

By using the orthogonality relation [Eq. (44)] and the expansions described above

$$v_x(k) = \sum_j v_j F_j(k), \quad (49)$$

$$\epsilon_k = \frac{\pi k_B T}{\sqrt{3}} \sigma_1(\epsilon_k), \quad (50)$$

$$\phi_k = \sum_{jk} \phi_{jn} F_j(k) \frac{\sigma_n(\epsilon_k)}{N(0)}, \quad (51)$$

$$Q_{kk'} = \sum_{jn'j'n'} Q_{jn'j'n'} F_j(k) \sigma_n(\epsilon_k) \left( -\frac{\partial f}{\partial \epsilon_k} \right) \\ \times F_{j'}(k') \sigma_{n'}(\epsilon_{k'}) \left( -\frac{\partial f}{\partial \epsilon_{k'}} \right), \quad (52)$$

Eqs. (2)–(4) can be transformed into

$$j_E = -2e \sum_j \phi_{j0} v_j, \quad (53)$$

$$j_Q = 2\pi \frac{k_B T}{\sqrt{3}} \sum_j \phi_{j1} v_j, \quad (54)$$

and

$$\alpha_{\text{out}}^2(jj'; \omega) F(\omega) = \delta_{jj'} \frac{\Omega_a^2}{(2\pi)^6} \int_j \frac{dS_k}{\hbar v_k} \frac{v_x^2(k)}{v_j^2} \int_{k'} \frac{dS_{k'}}{\hbar v_{k'}} \sum_i |M_{kk'}^i|^2 \delta(\omega - \omega_{k-k'}^i), \quad (60)$$

$$\alpha_{\text{in}}^2(jj'; \omega) F(\omega) = \frac{\Omega_a^2}{(2\pi)^6} \int_j \frac{dS_k}{\hbar v_k} \frac{v_x(k)}{v_j} \int_{j'} \frac{dS_{k'}}{\hbar v_{k'}} \frac{v_x(k')}{v_{j'}} \sum_i |M_{kk'}^i|^2 \delta(\omega - \omega_{k-k'}^i). \quad (61)$$

The frequency-dependent functions  $G_{nn'}^{\text{out}(\text{in})}(x)$  (where  $x = \hbar\omega/2k_B T$ ) are given by

$$G_{nn'}^{\text{out}(\text{in})} \left( \frac{\hbar\omega}{2k_B T} \right) = \frac{\hbar\omega}{2(k_B T)^2} \int_{-\infty}^{\infty} d\epsilon \int_{-\infty}^{\infty} d\epsilon' g(\epsilon, \epsilon', \omega) \sigma_n(\epsilon) \sigma_{n'}(\epsilon') = (x^2/\sinh^2 x) I_{nn'}^{\text{out}(\text{in})}(x). \quad (62)$$

The polynomials  $I_{nn'}^{\text{out}(\text{in})}(x)$  are simply related to similar polynomials denoted  $I_{nn}^+$  and  $I_{nn}^-$  by Allen<sup>11</sup> and Pinski<sup>12</sup>;  $I_{nn}^{\text{out}} = I_{nn}^+ + I_{nn}^-$  and  $I_{nn}^{\text{in}} = I_{nn}^+ - I_{nn}^-$ . The functions  $G_{nn'}^{\text{out}(\text{in})}(x)$  are universal functions independent of the material under consideration. At high  $T$  (small  $x$ ) the polynomials  $I_{nn}$  approach  $\delta_{nn}$ , which makes the scattering operator [Eq. (59)] diagonal in  $nn'$  with corrections of order  $(\Theta_D/T)^2$ . Thus to order  $(\Theta_D/T)^2$  the high- $T$  transport coefficients are not affected by  $\epsilon$  dependence of  $\phi$ , at least within our approximation of neglecting Fermi smearing.

$$\left( eE\delta_{n0} + \frac{\pi k_B}{\sqrt{3}} \frac{dT}{dx} \delta_{n1} \right) v_j = - \sum_{j'n'} Q_{jn'j'n'} \phi_{j'n'} \quad (55)$$

Thus, the Boltzmann equation has been converted into a matrix equation which is easily solved by inverting the scattering operator  $Q_{jn'j'n'}$  which from Eqs. (52) and (44) may be written

$$Q_{jn'j'n'} = \sum_{kk'} F_j(k) \sigma_n(\epsilon_k) Q_{kk'} F_{j'}(k') \frac{\sigma_{n'}(\epsilon_{k'})}{N^2(0)}. \quad (56)$$

The equations for  $\sigma$  and  $\kappa$  in this basis are

$$\sigma = 2e^2 \sum_{jj'} [Q^{-1}]_{j0j'} \sigma v_j v_{j'}, \quad (57)$$

and

$$\kappa = \frac{2\pi^2}{3} k_B^2 T \sum_{jj'} [Q^{-1}]_{j1j'} \sigma v_j v_{j'}. \quad (58)$$

The expression for  $Q_{jn'j'n'}$  [Eq. (56) can be developed in a manner analogous to our treatment of the LOVA in Sec. II. The scattering operator is written as a sum of scattering-out and scattering-in terms, and Fermi smearing is neglected, allowing  $Q_{jn'j'n'}^{\text{out}(\text{in})}$  to be written in terms of generalized spectral functions  $\alpha_{\text{out}(\text{in})}^2(jj'; \omega) F(\omega)$  and frequency-dependent functions  $G_{nn'}^{\text{out}(\text{in})}(\hbar\omega/2k_B T)$ ,

$$Q_{jn'j'n'}^{\text{out}(\text{in})} = \frac{2\pi k_B T}{\hbar N^2(0)^2} \int \frac{d\omega}{\omega} \alpha_{\text{out}(\text{in})}^2(jj'; \omega) F(\omega) G_{nn'}^{\text{out}(\text{in})}(x), \quad (59)$$

where the sheet-decomposed spectral functions are given by

## B. Computational details

The sheet-decomposed spectral function  $\alpha_{\text{out}(\text{in})}^2(jj'; \omega) F(\omega)$  given by Eqs. (60) and (61) were calculated using the same techniques as were used in evaluating the full spectral functions  $\alpha_{\text{out}(\text{in})}^2(\omega) F(\omega)$ , the only difference being that the Fermi-surface integrals over  $k$  and  $k'$  in Eq. (40) were restricted to the appropriate sheets of the Fermi surface. Nb and Pd Fermi surfaces both have three significant sheets. For Pd, a tiny hole pocket at the  $L$  point does not occur in our Fermi

surface because we neglect spin-orbit coupling.

The functions  $G_{nn'}^{\text{out}(in)}(\hbar\omega/2k_B T)$  were evaluated using Eq. (62) and the techniques described in Ref. 12. Energy polynomials of order zero through ten were included. The scattering matrix  $Q_{jn'j'n'}$  was then calculated as a function of temperature using Eq. (59) and finally  $\sigma$  and  $\kappa$  were evaluated using Eqs. (57) and (58). Because  $G_{nn'}^{\text{out}(in)}$  (and consequently  $Q_{jn'j'n'}$ ) vanishes unless  $n$  and  $n'$  are either both even or both odd, the scattering matrix may be written in a block diagonal form which makes it apparent that only the even (odd) energy polynomials enter the expression for the electrical (thermal) conductivity.

### C. Results with an anisotropic and energy-dependent distribution function

Below  $\sim 100$  K in Nb and Pd, we find that the distribution function  $\phi_k$  takes advantage of its variational flexibility to enhance the currents significantly. We illustrate separately the enhancement due to anisotropy (variation with  $k$  in the Fermi surface) and energy dependence (variation perpendicular to the Fermi surface) of  $\phi_k$ .

Our calculations permit anisotropy only to the extent that different sheets of Fermi surface are allowed to displace by different amounts. We call this the “ $N$ -sheet” model. The results for  $\rho$  and  $W$  (denoted  $\rho_N, W_N$ ) as a function of  $T$  are shown in Fig. 4. To clarify the effect of anisotropy, these are shown as ratios of the LOVA results, where all sheets are constrained to displace the same amount. Three features stand out: (a) the effect is small above 50 K, (b) the effect is larger in Pd than Nb, and (c) a qualitative but not quantitative Wiedemann-Franz scaling is obeyed. The proportionality of  $\rho$  to  $WT$  has already failed at these temperatures because of inelastic scattering. Nevertheless, it is instructive to observe that the enhancement of  $\sigma$  due to anisotropy is quite similar to the enhancement of  $\kappa$ , but strict numerical equality of these enhancements does not occur (nor does theory tell us to expect it.)

Observation (a), the smallness of the anisotropy enhancement above 50 K, needs some cautionary remarks. An approximate formula for the enhancement for  $T \geq \theta_D$  can be worked out as follows. We have already remarked that at high  $T$ , scattering in is small compared to scattering out. If we neglect scattering in, the Boltzmann equation is no longer an integral equation and the exact solution for  $\sigma$  is

$$\sigma_{\text{out}} = \frac{2}{3} e^2 \sum_k v_k^2 \tau_k \left( \frac{-\partial f}{\partial \epsilon_k} \right), \quad (63)$$

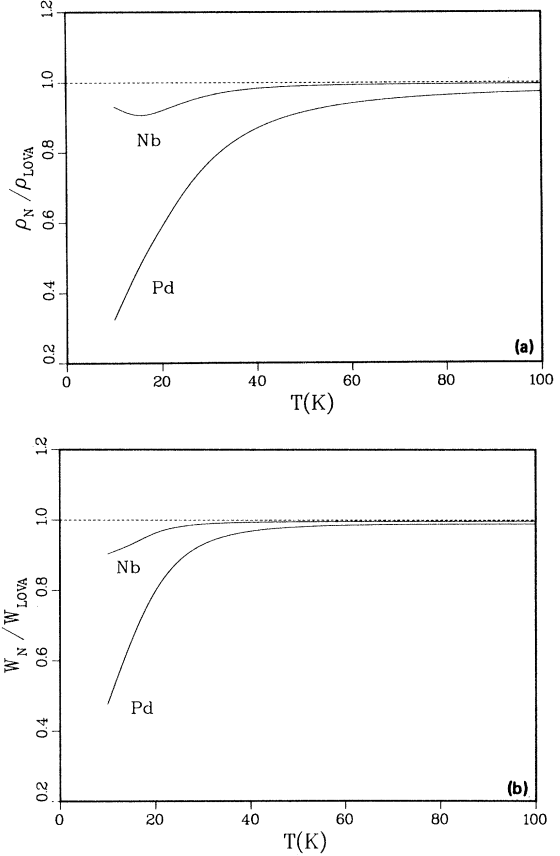


FIG. 4. The effect on the electrical and thermal resistivities of Nb and Pd of allowing intersheet variations in the distribution function.  $\rho_N$  and  $W_N$  are the electrical and thermal resistivities in the  $N$ -sheet approximation.  $\rho_{\text{LOVA}}$  and  $W_{\text{LOVA}}$  are the resistivities calculated in lowest-order variational approximation using a realistic spectral function.

where  $\tau_k$  is the “quasiparticle lifetime” which at high temperatures is  $\hbar/2\pi\lambda_k k_B T$ , and  $\lambda_k$  is the mass enhancement. Let us define an average denoted by  $\langle \rangle_{\text{av}}$ ,

$$\langle A \rangle_{\text{av}} \equiv \frac{\sum_k v_k^2 A_k \left( \frac{-\partial f}{\partial \epsilon_k} \right)}{\sum_k v_k^2 \left( \frac{-\partial f}{\partial \epsilon_k} \right)}. \quad (64)$$

Thus, the “exact” answer [Eq. (63)] is proportional to  $\langle 1/\lambda \rangle_{\text{av}}$ , whereas, if we use LOVA and discard scattering in, the result is proportional instead to  $1/\lambda_{\text{out}} = 1/\langle \lambda \rangle_{\text{av}}$ . Thus, the enhancement of  $\sigma$  due to anisotropy is

$$\delta\sigma/\sigma_{\text{LOVA}} \langle \lambda \rangle_{\text{av}} \langle 1/\lambda \rangle_{\text{av}} - 1 \cong \langle (\delta\lambda)^2 \rangle_{\text{av}} / \langle \lambda^2 \rangle_{\text{av}} \quad (T \geq \theta_D), \quad (65)$$

where the last equality is valid for weak anisotropy, i.e., if  $\delta\lambda = \lambda_k - \langle \lambda \rangle_{\text{av}}$  is small compared to  $\lambda$ . There is a close analogy<sup>11</sup> with the theory

of anisotropy enhancement of the superconducting  $T_c$ .<sup>28</sup> Our high- $T$  enhancement is an effect of order 1%, corresponding to a  $\lambda$  anisotropy of  $\sim 10\%$ . Two comments need to be made. First, we underestimate the  $\lambda$  anisotropy by making the  $N$ -sheet model. Second,  $\lambda$  anisotropy has been studied by de Haas–van Alphen measurements,<sup>23</sup> and our rigid muffin-tin procedures give less anisotropy<sup>26,29</sup> than is estimated from experiment. Coleridge<sup>30</sup> has illustrated how the RMTA can give a good account of  $\langle \lambda \rangle_{av}$  but a poor account of  $\delta \lambda_k$ . Thus, for both reasons, the high- $T$  anisotropy enhancement of  $\sigma$  is probably larger than our calculation shows.

At low  $T$ , only small- $\omega$  phonons can scatter electrons, which means that scattering events go increasingly into nearby  $\vec{k}$  states as  $T$  is lowered. At  $k_B T \ll \hbar v q_{min}$ , where  $q_{min}$  is the minimum wave vector coupling different sheets of Fermi surface, the different sheets become decoupled. Anisotropy effects are greater at low  $T$ , partly because the large momentum transfers available at high  $T$  tend to average out anisotropy and partly because at small  $q$ , the phonon dispersion is particularly anisotropic. We can now explain observation (b), that the low- $T$  anisotropy enhancement is particularly large in Pd. The  $\Gamma$ -centered sheet in Pd has large velocities and thus a small  $N_j(0)$  [only 8% of the total  $N(0)$ ]. Thus, when sheets become decoupled, the quasiparticle lifetime  $\tau_j$  for  $\Gamma$ -sheet electrons becomes particularly large, due to the low density of states available for scattering processes. Also, the cancellation of scattering in against scattering out is more effective for  $\Gamma$ -sheet electrons because the curvature of this surface is smaller, making  $\vec{v}_k \cdot \vec{v}_k$  closer to  $v_k^2$  for fixed small  $\vec{k} - \vec{k}'$ . Figure 5 plots the lifetimes of each sheet normalized to the mean lifetime. Below 30 K there is a dramatic increase of the  $\Gamma$ -sheet lifetime in Pd, showing that sheets are becoming decoupled. In Nb, where the different sheets have velocities which are all roughly comparable, the effect is smaller. A further discussion of these effects is given in Sec. IV where we make a critical analysis of the “ $s$ - $d$ ” model.

We now consider the additional enhancement coming from energy dependence. Figure 6 shows the results,  $\rho_{CF}$  and  $W_{CF}$  where CF denotes that the complete energy dependence is extracted by continued fraction extrapolations based on the first 10 energy polynomials. The results  $\rho_{CF}$  and  $W_{CF}$  contain *both* anisotropy and energy dependence and are shown normalized to  $\rho_N$  and  $W_N$ , the results with anisotropy but without energy dependence. Two of the three observations made in connection with Fig. 4 apply also here. First,

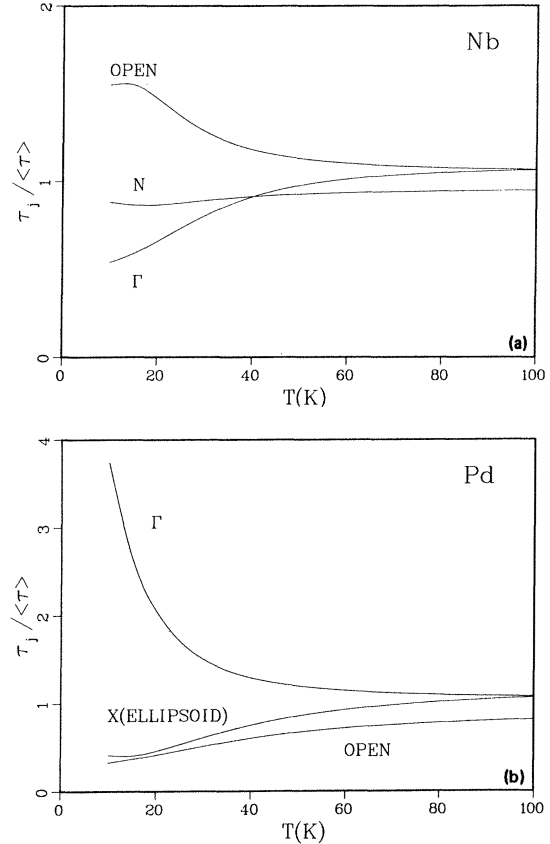


FIG. 5. Lifetimes for electrons on different Fermi surface sheets of Nb and Pd.  $\tau_j$  is the average lifetime of electrons on sheet  $j$  due to scattering-out processes.  $\langle \tau \rangle$  is the average over all sheets of the scattering-out lifetime.

there is qualitative but not quantitative Wiedemann-Franz scaling. This observation would be less applicable if we had results below 10 K, as is clear from Ref. 12. In the isotropic case (single spherical sheet)  $\rho_{CF}/\rho_{LOVA}$  must go back to 1 at  $T=0$ , whereas  $W_{CF}/W_{LOVA}$  goes to  $\sim 0.66$ . When anisotropy is included, these effects interact, and simple  $T=0$  limits do not arise. Second, the enhancement of  $\sigma$  and  $\kappa$  due to energy dependence goes away at high  $T$ . This was explained in Sec. III A. The enhancement occurs because when there is inelasticity in the scattering,  $\phi_k$  can take advantage of its variational freedom as a function of  $\epsilon_k$  to maximize the currents. As  $T$  becomes  $\geq \Theta_D$ , the inelasticity becomes increasingly unimportant. Unlike Fig. 4, the enhancement in Fig. 6 is nearly the same in Nb and Pd. Pinski<sup>12</sup> showed in the isotropic case that the enhancement depends on a parameter  $(k_F/q_D)^2$  which determines the relative strength of  $\alpha_{out}^2(\omega)F(\omega)$  and  $\alpha_{tr}^2(\omega)F(\omega)$ . For both Pd and Nb the corresponding parameter in the series expansions [Eqs. (30) and (31)],

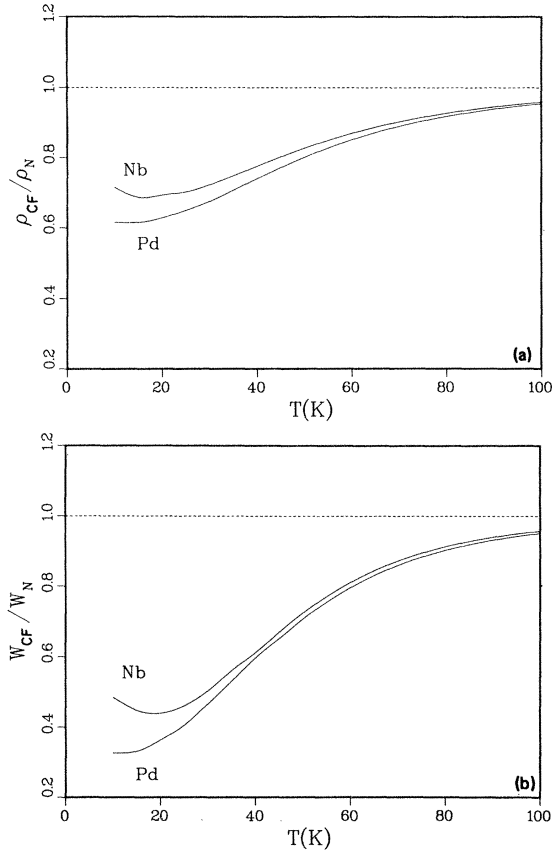


FIG. 6. Effect on the electrical and thermal resistivities of Nb and Pd of allowing the distribution function  $\phi_X$  to be energy dependent.  $\rho_{CF}$  and  $W_{CF}$  are the electrical and thermal resistivities calculated using an energy polynomial expansion for the distribution function with a continued-fraction extrapolation to approximate the limit of an infinite number of energy polynomials.  $\rho_{CF}$  and  $W_{CF}$  contain effects of energy dependence and sheet-to-sheet variations of the distribution function; only the sheet-to-sheet variations are contained in  $\rho_N$  and  $W_N$ .

namely,  $(\lambda_{out}\langle\omega^2\rangle_{out}/3\lambda_{tr}\langle\omega^2\rangle_{tr})^{1/2}$  is approximately  $1/\sqrt{3}$  and this probably quite generally true in  $d$ -band metals, suggesting that enhancement due to energy dependence may be only weakly dependent on details specific to the material.

#### D. Comparison with experiment

In Figs. 7 and 8, we compare our calculated electrical and thermal resistivities with experiment. The experimental data are from Webb<sup>31</sup> (Nb  $\rho$ ), Ho *et al.*<sup>32</sup> (Nb  $W$  and Pd  $W$ ), Moore *et al.*<sup>33</sup> (Nb  $W$ ), and Williams and Weaver<sup>34</sup> (Pd  $\rho$ ). The electrical resistivities near room temperature are in good agreement with experiment. Theory (dashed) exceeds experiment (solid) by about 10% for both Nb and Pd.

In comparing the calculated thermal resistivities with experiment one should allow for the heat

current carried by the phonons. The lattice thermal conductivity of Nb has been estimated by Moore *et al.*<sup>33</sup> from measurements on a series of dilute alloys. Their values for the *electronic* thermal resistivity allowing for the lattice thermal current are shown in Fig. 7(b) ( $\times$ 's). We have corrected the Nb and Pd thermal-conductivity data of Ho *et al.*<sup>32</sup> for the lattice thermal current using<sup>35</sup>

$$(\kappa_p)^{-1} = A(\Theta/T)^2 J_3^{-1}(\Theta/T) + BT, \quad (66)$$

where the first term describes a lattice thermal resistance due to phonon decay into electron-hole pairs and the second term arises from phonon-phonon scattering. We estimate  $A = 11$  K cm/watt,  $B = 0.02$  cm/watt for Nb and  $A = 2.9$  K cm/watt,  $B = 0.04$  cm/watt for Pd. The effect of correcting for the lattice conductivity is to increase the experimental electronic thermal resistivity by about 6% for Nb and about 14% for Pd over the temperature range 100–300 K. With these corrections to the experimental data the electrical and thermal resistivities form a consistent picture at temperatures in the 100–300 K range. The calculated electrical and thermal resistivities are slightly high (~10%) for both Nb and Pd.

The overestimate of 10% probably derives from two uncertain aspects of the theory: first, the rigid muffin-tin model, and second, the more fundamental question of whether the band structure we use gives correctly the quasiparticle energies needed for transport theory. This second question seems at the moment difficult to settle. The fact that our calculation agrees with experiment to within 10% suggests that the band structure is quite good for transport properties, unless there is a degree of cancellation of errors from the two sources. A third possible source of error is our neglect of Fermi smearing. This effect is quite important at higher temperatures in these materials and is responsible<sup>5,36-38</sup> (together with anharmonicity in Nb) for substantial negative deviations from linearity in the resistivity. These deviations are readily detectable above about 500 K in both materials and may be important at 300 K.

From 30 to 100 K there is good agreement between theory and experiment for both materials. (We prefer the data of Moore *et al.* for the Nb thermal resistivity.) At lower temperatures (10–20 K), however, it appears (especially for Nb) that the calculated values of the resistivity are lower than the measured ones. The comparison between theory and experiment is complicated in this temperature range by impurity scattering and by the possibility of electron-electron and

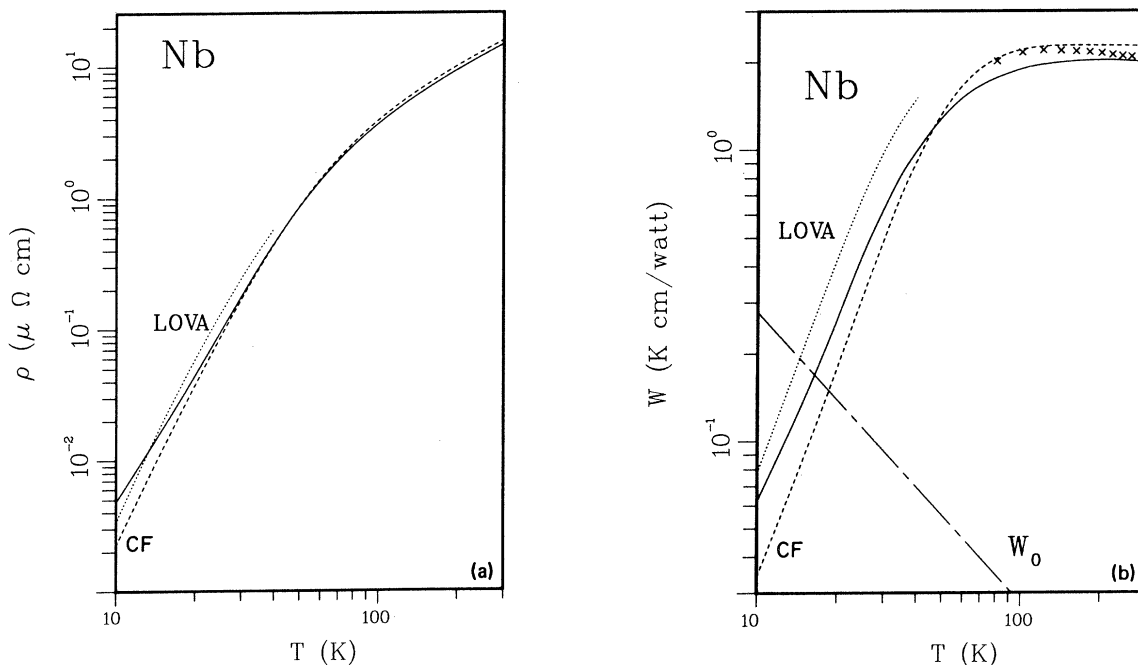


FIG. 7. Calculated electrical and thermal resistivities of Nb compared with experiment. Dotted curves were calculated in lowest-order variational approximation using realistic spectral functions. Dashed curves labeled CF are our "best" solutions to the Boltzmann equation. Solid curves and  $\times$ 's are experiment (Refs. 31–33). Impurity resistivities have been subtracted from the experimental curves.  $W_0$  is the thermal resistivity due to impurity scattering. The residual electrical resistivity for the data of (a) is  $0.75 \times 10^{-3} \mu\Omega \text{ cm}$ . The experimental thermal resistivity (Ref. 32, shown as the solid line) has been corrected for the thermal current carried by the lattice [Eq. (66)]. The data of Ref. 33 (shown as  $\times$ 's) had already been corrected.

electron-paramagnon scattering in Pd.

Impurity scattering effectively increases the electron-phonon resistivity because the distribution function cannot simultaneously adjust to take full advantage of both types of scattering anisotropy simultaneously. A careful treatment of this effect would require a detailed knowledge of the types and concentrations of the impurities and other lattice imperfections and is beyond the scope of this paper. Qualitatively, we expect the electron-phonon resistivity to rise above  $\rho_{CF}(T)$  as impurity scattering becomes important and to approach a value comparable to  $\rho_{LOVA}$  in the impurity-dominated regime.

For Webb's sample, the impurity resistivity  $\rho_0$  was very small ( $0.75 \times 10^{-3} \mu\Omega \text{ cm}$ ) and should not affect the electron-phonon resistivity above 10 K. Thus, it appears from Fig. 7(a) that the calculation underestimated the strength of the electron-phonon scattering at low temperatures. It should be noted that a better solution to the Boltzmann equation could only lower  $\rho_{CF}(T)$ . The most likely source of this discrepancy between theory and experiment is again our use of rigid

muffin-tin matrix elements. The only way of avoiding this conclusion that we can see is to ascribe part of low-temperature resistivity to electron-electron or electron-paramagnon scattering. Since the experimental resistivity<sup>31</sup> varies as  $T^3$  rather than as  $T^2$  at low temperatures, this interpretation is somewhat strained. One of us<sup>4</sup> has listed evidence from several sources that the rigid muffin-tin matrix elements are too weak for low momentum transfer, although Ruesink *et al.*<sup>39</sup> reached a different conclusion from an analysis of the effects of shear strains on de Haas–van Alphen orbits.

The interpretation of the low-temperature resistivity of Pd is even more complicated. Figures 8(a) and 8(b) show the calculated and experimental values of the electrical and thermal resistivities. Impurity resistivities,  $\rho_0$  ( $\propto T^0$ ) and  $W_0$  ( $\propto T^{-1}$ ) have been subtracted from the experimental electrical and thermal resistivities, respectively. At first glance, the calculated resistivities appear to be in reasonable agreement with experiment at low temperature. The resistivities follow  $\rho_{CF}$  and  $W_{CF}$  above  $\rho_0$  and

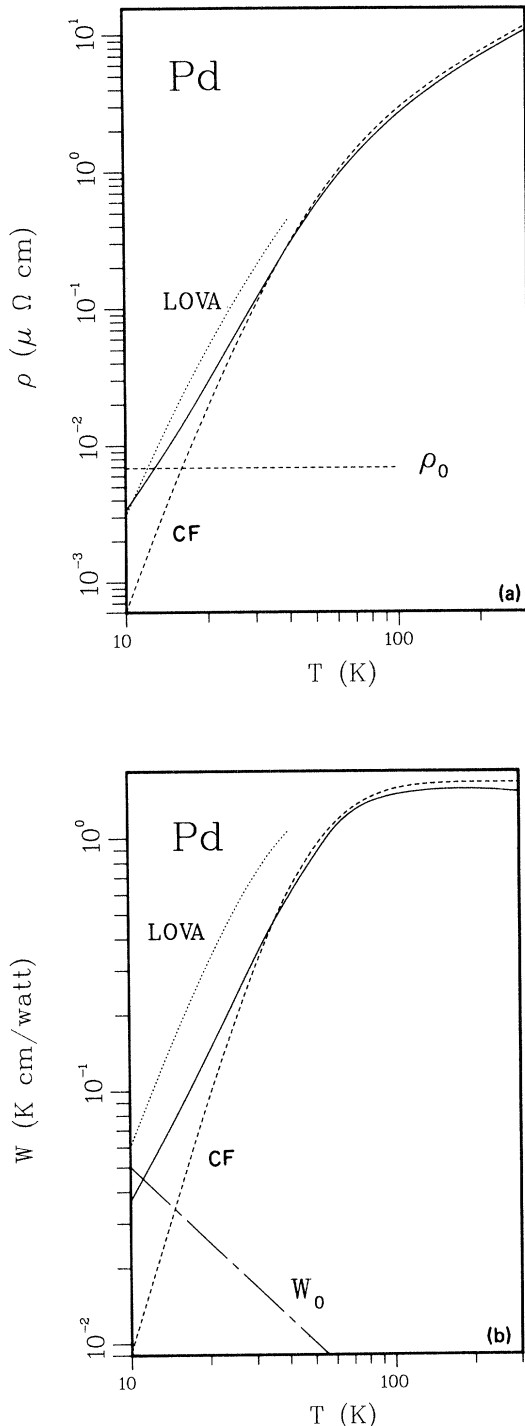


FIG. 8. Calculated electrical and thermal resistivities of Pd compared with experiment. Dotted curves are calculated in LOVA. Dashed curves are our "best" solution to the Boltzmann equation. The solid curves are the experimental data (Refs. 32 and 34) after correction for impurity scattering and in the case of the thermal resistivity for the lattice thermal current.  $\rho_0$  and  $W_0$  denote the electrical and thermal impurity resistivities.

$W_0$ , respectively but lie above the CF curves at lower temperatures approaching the LOVA results, as expected, in the impurity-dominated regime. This interpretation is probably not correct, however, since the temperature-dependent part of the electrical resistivity is dominated below 10 K by a term proportional to  $T^2$  which lies well above any reasonable extrapolation of the calculated electron-phonon electrical resistivity to lower temperatures.

This  $T^2$  term and a corresponding term proportional to  $T$  in the thermal resistivity have received much attention.<sup>40-45</sup> High-precision measurements using superconducting quantum-interference devices (SQUID's) have established that the temperature dependence of the electrical resistivity of Pd is accurately given by

$$\rho(T) = \rho_0 + AT^2, \quad (67)$$

below 5 K. The magnitude of  $A$ , however, appears to be sample dependent. Webb *et al.*<sup>45</sup> determined  $A$  to be  $1.59 \times 10^{-11} \Omega \text{ cm/K}^2$  for a very pure sample (residual resistivity ratio of 22 500) while Uher and Schroeder<sup>43</sup> found  $A$  to be  $3.48 \times 10^{-11} \Omega \text{ cm/K}^2$  in a sample with a residual resistance ratio of 1127. The higher value of  $A$  is typical of values obtained using standard four-probe techniques to measure the resistivity.<sup>41,42,46</sup> Schindler and Rice<sup>40</sup> found that small amounts of Ni cause both the susceptibility  $\chi$  and the coefficient to increase dramatically, whereas Greig and Rowlands<sup>42</sup> found that most impurities cause  $A$  to decrease. Still, it is difficult to reconcile the different values of  $A$  obtained in Refs. 43 and 45.

Since the  $T^2$  term in the electrical resistivity is usually attributed to electron-electron or electron-paramagnon scattering, we would like to subtract it from the experimental data so that we can compare the remainder with the calculated electron-phonon resistivity. The data show that  $T^2$  behavior cannot be assumed to persist at high temperature. Using the higher value of  $A$ , the  $T^2$  term amounts to 30% of the observed electrical resistivity at 300 K and would exceed it above 1000 K. If we use the smaller value of  $A$ , the  $T^2$  term exceeds the observed resistivity above 1700 K. Fermi smearing (and also possible "saturation" effects<sup>47</sup> associated with short mean free paths) complicated the analysis of the resistivity of Pd above 500 K, but even below 500 K it is clearly necessary to abandon Eq. (67).

One way to resolve the problem is to attribute the  $T^2$  term to scattering from spin fluctuations, and to assume a relatively low spin-fluctuation temperature. Using a simple approximation for the spin-fluctuation (SF) spectral function, Schind-

ler and Rice<sup>40</sup> derived a temperature dependence of the spin-fluctuation resistivity of the form

$$\rho_{\text{SF}}(T) = \alpha (T/\Theta_{\text{SF}})^2 [J_2(\Theta_{\text{SF}}/T) - (T/\Theta_{\text{SF}})^3 J_5(\Theta_{\text{SF}}/T)], \quad (68)$$

with  $\Theta_{\text{SF}}$  of the order 200 K. In Fig. 9, we again compare theory to experiment but in this case we have subtracted from the experimental resistivity not only  $\rho_0$  but also  $\rho_{\text{SF}}$  is given by Eq. (68). The spin-fluctuation temperature was assumed to be 190 K, the value obtained by extrapolating the spin-fluctuation temperatures of Pd(Ni) alloys<sup>40</sup> to zero Ni concentration. The coefficient  $\alpha$  was chosen to be  $0.174 \mu\Omega \text{ cm}$ , a value which corresponds to  $A = 1.59 \times 10^{-11} \Omega \text{ cm/K}^2$  in Eq. (67). This value of  $A$  agrees with the value obtained on the purest sample available<sup>45</sup> and gives a good fit to the low-temperature data of Williams and Weaver which we are using. The agreement between theory and experiment seems quite reasonable at all temperatures.

We have considered two alternate ways to resolve the problem of the "missing" high- $T$   $T^2$  resistivity of Pd. First, "Fermi smearing" has a large effect<sup>5</sup> on  $\rho(T)$  above 500 K, and acts to diminish the electron-phonon resistivity. It seems

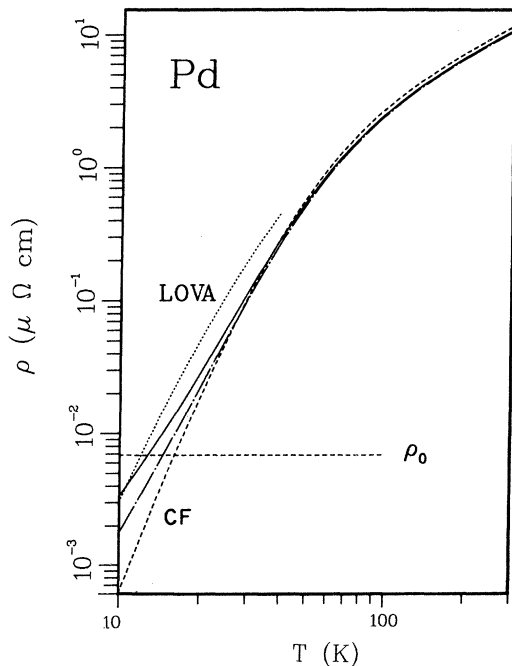


FIG. 9. Calculated electron-phonon resistivity (dashed and dotted lines) of Pd compared with experiment. The solid line is experiment (Ref. 34) with  $\rho_0$  subtracted as in Fig. 8(a). The dot-dashed line is experiment with electron-paramagnon scattering subtracted using Eq. (68).

possible that Coulomb scattering would be even more strongly reduced by Fermi smearing because it is more sensitive to electronic density of states. Second, "saturation" of  $\rho(T)$  is known to occur in  $d$ -band compounds<sup>47</sup> when the mean free path  $l$  approaches unit-cell dimensions  $a$ . There is possible<sup>37</sup> but not definitive<sup>38</sup> evidence for "saturation" in Nb for  $T < 1000$  K. Because of the small Fermi velocities in Pd (Table I) the values of  $l/a$  are not large and "saturation" is a possible effect. Consistent with this possibility, the resistivity of Pd can be quite nicely fitted by a "shunt-resistor model"  $\rho^{-1} = \rho_{\text{Boltz}}^{-1} + \rho_{\text{max}}^{-1}$  as used for A15 metals,<sup>47</sup> where the Boltzmann resistivity  $\rho_{\text{Boltz}}$  is equal to our calculated electron-phonon part plus Eq. (67), and  $\rho_{\text{max}}$  is  $\sim 70 \mu\Omega \text{ cm}$ . The idea here is that the  $T^2$  term is "missing" at high  $T$  not because it goes away [as in Eq. (68)], but because it is hidden by "saturation." However, the value  $\rho_{\text{max}} \approx 70 \mu\Omega \text{ cm}$  is smaller by 2 than in metals where "saturation" is more clearly documented. Thus we prefer the paramagnon explanation. The fact that  $A$  is larger in Pd than in Nb, that it increases dramatically with Ni impurities and scales with  $\chi$ , and that superconductivity is suppressed in Pd, all argue for a special "paramagnon" effect with a reasonably small characteristic temperature  $\Theta_{\text{SF}}$ . Even accepting this explanation, the details of Eq. (68) are not to be trusted, and substantial uncertainty remains. It is surprising how well electron-phonon effects alone seem to account for the data above 10 K as shown in Fig. 7(a).

#### IV. CONCLUSIONS

To summarize, the overall agreement with experimental transport coefficients in Nb and Pd is very good. This, combined with the successes in predicting linewidths of phonons,<sup>6-8</sup> provides strong confirmation of the RMTA, and a clear demonstration of the applicability of the Bloch-Boltzmann theory of transport to transition elements. The fact that we underestimate  $\rho$  at low  $T$  in Nb can be interpreted as possible evidence that RMTA is wrong<sup>4</sup> at small  $q$  in Nb.

Our results illustrate quite vividly the inadequacy of simple model theories for understanding details of  $T$  dependence in these metals. The Bloch-Grüneisen formula  $\rho \sim T^5 J_5(\Theta/T)$  and the corresponding formula for  $W$  capture the correct overall shape of  $\rho(T)$  but make many unrealistic assumptions and approximations. These show up as strong departures in our results from the simple BG behavior. There is an accidental tendency for some of these departures to cancel *partially*. The corrections to BG behavior are of two types, improvements in the model and im-

improvements in the solution of the Boltzmann equation. The use of realistic energy bands, phonons, and coupling matrix elements, leads to significant changes in the LOVA solutions for  $\rho$  and  $W$ . The LOVA represents the same level of mathematical approximation as BG theory does in solving the Boltzmann theory. The more realistic LOVA results have a higher  $\rho$  at low  $T$ , and a lower  $L_0W - \rho/T$ , for Nb, Pd, and no doubt most other metals. However, it is very important to seek improved solutions of the Boltzmann theory, which will reduce the predicted  $\rho$  and  $W$  (this is where partially cancelling errors can accidentally make BG theory look better than it is). The enhancement of  $\sigma$  and  $\kappa$  due to scattering anisotropy on the Fermi surface is difficult to calculate well, and our  $N$ -sheet model represents a first attempt. The enhancement due to  $\epsilon_k$  dependence of the distribution function can now be regarded as a solved problem,<sup>11, 12, 27</sup> and we have fully accounted for this effect. Both types of enhancement will be altered by impurity scattering, leading to large deviations from Mattheissen's rule (DMR) at temperatures  $T \lesssim 80$  K. Such effects have been seen in dilute Pd alloys by Azabar and Williams<sup>48</sup> and by Williams and Weaver.<sup>49</sup> Theory thus tells us that low- $T$  resistivity should not obey any simple theory and should be highly sensitive to impurity concentration. In particular, the low- $T$  power law is still, in principle,  $T^5$  (neglecting Coulomb scattering and phonon drag) but the temperature range where  $T^5$  should be obeyed is drastically reduced even in LOVA, and will be further altered by anisotropy enhancement effects and DMR.

It is worth giving special mention to the "s-d" model. Originally, it was given by Mott<sup>50</sup> as a model for Pd and Ni. He supposed there were two sheets of Fermi surface, containing slow and fast ( $d$  and  $s$ , respectively) electrons. The  $s$  electrons, being fast, would carry most of the current. Since the  $d$  density of states is large, the dominant scattering would be  $s$  to  $d$ . Our results for Pd agree qualitatively with this picture. The fast electrons are on the  $\Gamma$ -centered sheet (which is dominantly  $d$ - rather than  $s$ -like in character, but this does not alter the physics, only the names). The slow electrons are on the jungle gym; other pieces of Fermi surface are not significant. In LOVA, the  $\Gamma$  electrons carry 73% of the current, even though only 8% of the density of states resides there. Scattering is dominantly from the  $\Gamma$  sheet to the jungle gym. In the more realistic  $N$ -sheet approximation, the  $\Gamma$ -centered sheet carries even a larger fraction of the current, up to 97% at 10 K. Nb, on the other hand, has no sheet of fast electrons, and the  $s$ - $d$  model does not apply even qualitatively.

Further mathematical development of this model was given by Wilson<sup>35</sup> who proposed that this model should give an extra term in the resistivity proportional to  $T^3 J_3(\Theta/T)$ , but reduced by  $e^{-E_{\min}/kT}$  where  $E_{\min} = \hbar v_s q_{\min}$  is the minimum phonon energy necessary to scatter from an "s" sheet to a "d" sheet. Subsequently, many authors have kept the  $T^3 J_3(\Theta/T)$  part, but dropped the exponential reduction. We find no justification for either of these in Pd. A  $T^3$  law requires that spectral functions remain Debye-type for frequencies  $\omega$  considerably higher than  $v_s q_{\min}$ , whereas we find the Debye tail to occur only at low  $\omega$ . Behavior close to  $T^3$  has been found by Webb<sup>31</sup> in Nb. This appears accidental to us. We can assert with confidence that it has nothing to do with "s-d" scattering.

This brings us to our final point, the significance of fitting data to simple formulas. Obviously, it is pleasing to have a simple fit, and a power series in  $T$  is logical to try at low  $T$ . However, great caution is needed when assigning an interpretation to such a fit. Suppose the form  $a + bT^2 + cT^n$  works where  $n$  is typically 3 or 5. The coefficient  $b$  may measure the strength of electron-electron (Coulomb or spin-fluctuation) scattering. However, to be confident of this, one must verify that  $b$  varies only weakly with  $a$ , as different samples are measured, and also high enough purity should be attempted so that  $bT^2$  exceeds both  $a$  and  $cT^n$  for a decent temperature interval. Experiments on Pd come close to satisfying these tests but there is need for further work to confirm electron-electron scattering. Similar comments apply if an assignment is to be made to the coefficient  $c$ . The power-series fit will, of course, cover only the low- $T$  region. In order to fit a wider region, it is common to multiply  $T^n$  by  $J_n(\Theta/T)$ , which permits a smooth interpolation between  $T^n$  for  $T \leq \Theta$  and  $T^1$  for  $T \geq \Theta$ . We see no reason to discourage this practice, except for the problem that such a fit suggests an unwarranted interpretation. We strongly suggest that the function  $J_n$  should be regarded as only an interpolation function.

#### ACKNOWLEDGMENTS

Work at Stony Brook was supported in part by National Science Foundation Grant No. DMR79-00837. Work at Oak Ridge is sponsored by the Division of Materials Science, with the U. S. Department of Energy under Contract No. W-7405-eng-26 with the Union Carbide Corporation. We thank R. K. Williams for advice and encouragement, and for permission to use data produced by the Physical Properties Group at ORNL prior to publication.

- \*Present address: General Electric Research and Development Center, Schenectady, New York 12301.
- <sup>1</sup>F. Bloch, *Z. Phys.* **52**, 555 (1928).
  - <sup>2</sup>J. Yamashita and S. Asano, *Prog. Theor. Phys.* **51**, 317 (1974).
  - <sup>3</sup>R. C. Shukla and R. Taylor, *J. Phys. C* **6**, 531 (1976).
  - <sup>4</sup>W. H. Butler, in *Physics of Transition Metals, 1980*, edited by P. Rhodes (Institute of Physics, London, 1981), pp. 505–514.
  - <sup>5</sup>F. J. Pinski, P. B. Allen, and W. H. Butler, *Phys. Rev. Lett.* **41**, 431 (1978).
  - <sup>6</sup>W. H. Butler, H. G. Smith, and N. Wakabayashi, *Phys. Rev. Lett.* **39**, 1004 (1977).
  - <sup>7</sup>W. H. Butler, F. J. Pinski, and P. B. Allen, *Phys. Rev. B* **19**, 3708 (1979).
  - <sup>8</sup>F. J. Pinski and W. H. Butler, *Phys. Rev. B* **19**, 6010 (1979).
  - <sup>9</sup>W. H. Butler, in *Superconductivity in d- and f-Band Metals*, edited by H. Suhl and M. B. Maple (Academic, New York, 1980), pp. 443–453.
  - <sup>10</sup>D. Glötzel, D. Rainer, and H. Schober, *Z. Phys. B* **35**, 317 (1979).
  - <sup>11</sup>P. B. Allen, *Phys. Rev. B* **17**, 3725 (1978).
  - <sup>12</sup>F. J. Pinski, *Phys. Rev. B* **21**, 4380 (1980).
  - <sup>13</sup>J. M. Ziman, *Electrons and Phonons* (Oxford University Press, Oxford, 1960).
  - <sup>14</sup>F. J. Blatt, *Physics of Electronic Conduction in Solids* (McGraw-Hill, New York, 1968).
  - <sup>15</sup>T. Holstein, *Ann. Phys. (New York)* **29**, 410 (1964).
  - <sup>16</sup>D. J. Scalapino, in *Superconductivity*, edited by R. D. Parks (M. Dekker, New York, 1969), Vol. 1, pp. 449–500.
  - <sup>17</sup>W. L. McMillan, *Phys. Rev.* **167**, 331 (1968).
  - <sup>18</sup>F. Bloch, *Z. Phys.* **59**, 208 (1930).
  - <sup>19</sup>A. H. Wilson, *Proc. Cambridge Philos. Soc.* **33**, 371 (1937).
  - <sup>20</sup>J. S. Faulkner, H. L. Davis, H. W. Joy, *Phys. Rev.* **161**, 656 (1967).
  - <sup>21</sup>W. H. Butler, J. J. Olson, J. S. Faulkner, and B. L. Gyorffy, *Phys. Rev. B* **14**, 3823 (1976).
  - <sup>22</sup>G. Gilat and L. J. Raubenheimer, *Phys. Rev.* **144**, 390 (1966).
  - <sup>23</sup>G. W. Crabtree, private communication; G. W. Crabtree, D. H. Dye, D. P. Karim, D. D. Koelling, and J. B. Ketterson, *Phys. Rev. Lett.* **42**, 390 (1979).
  - <sup>24</sup>B. M. Powell, P. Martel, and A. D. B. Woods, *Can. J. Phys.* **55**, 1601 (1977).
  - <sup>25</sup>A. P. Müller and B. N. Brockhouse, *Can. J. Phys.* **49**, 704 (1971).
  - <sup>26</sup>F. S. Khan and P. B. Allen, *Phys. Status Solidi B* **100**, 227 (1980).
  - <sup>27</sup>H.-L. Engquist, *Phys. Rev. B* **21**, 2067 (1980).
  - <sup>28</sup>W. H. Butler and P. B. Allen, in *Superconductivity in d- and f-Band Metals*, edited by D. H. Douglass (Plenum, New York, 1976), pp. 73–120.
  - <sup>29</sup>F. J. Pinski and W. H. Butler, unpublished.
  - <sup>30</sup>P. T. Coleridge, unpublished.
  - <sup>31</sup>G. W. Webb, *Phys. Rev.* **181**, 1127 (1968); Webb's data is unnormalized, we use  $\rho(300\text{ K}) = 14.76\ \mu\Omega\text{ cm}$ .
  - <sup>32</sup>C. Y. Ho, R. W. Powell, and P. E. Liley, *J. Phys. Chem. Ref. Data* **3**, Suppl. 1, 470 (1974), (Nb); **3**, Suppl. 1, 502 (1974), (Pd).
  - <sup>33</sup>J. P. Moore, R. K. Williams, R. S. Graves, F. J. Weaver, F. J. Pinski, and W. H. Butler, Metals and Ceramics Division Materials Science Program Annual Progress Report No. ORNL-5672, unpublished, p. 139.
  - <sup>34</sup>R. K. Williams and F. J. Weaver, Metals and Ceramics Division Materials Science Program Annual Progress Report No. ORNL-5672 unpublished, p. 143.
  - <sup>35</sup>W. H. Butler and R. K. Williams, *Phys. Rev. B* **18**, 6483 (1978).
  - <sup>36</sup>F. Y. Fradin, *Phys. Rev. Lett.* **33**, 158 (1974).
  - <sup>37</sup>P. B. Allen, *Phys. Rev. Lett.* **37**, 1638 (1976).
  - <sup>38</sup>M. J. Laubitz, C. R. Leavens, and R. Taylor, *Phys. Rev. Lett.* **39**, 225 (1977).
  - <sup>39</sup>W. Ruesink, J. deWilde, R. Griessen, and M. J. G. Lee, *J. Phys. (Paris) Colloq.* **39**, C6-1097 (1978).
  - <sup>40</sup>A. I. Schindler and M. J. Rice, *Phys. Rev.* **164**, 759 (1967).
  - <sup>41</sup>J. T. Schriempf, *Phys. Rev. Lett.* **20**, 1034 (1968).
  - <sup>42</sup>D. Greig and J. A. Rowlands, *J. Phys. F* **4**, 232 (1974).
  - <sup>43</sup>C. Uher and P. A. Schroeder, *J. Phys. F* **8**, 865 (1978).
  - <sup>44</sup>P. A. Schroeder and C. Uher, *Phys. Rev. B* **18**, 3884 (1978).
  - <sup>45</sup>R. A. Webb, G. W. Crabtree, and J. J. Vuillemin, *Phys. Rev. Lett.* **43**, 796 (1979).
  - <sup>46</sup>G. K. White and S. B. Woods, *Philos. Trans. R. Soc. London* **251A**, 273 (1959).
  - <sup>47</sup>P. B. Allen, in *Superconductivity in d- and f-Band Metals*, Ref. 9, pp. 291–304; also in *Physics of Transition Metals, 1980*, Ref. 4, pp. 425–433.
  - <sup>48</sup>E. K. Azabar and G. Williams, *Phys. Rev. B* **14**, 3301 (1976).
  - <sup>49</sup>R. K. Williams and F. J. Weaver, Annual Progress Report, Metals and Ceramics Division, Report No. ORNL-5672, unpublished.
  - <sup>50</sup>N. F. Mott, *Proc. R. Soc. London Ser. A* **153**, 699 (1936).